AUTHOR(S): CHACRA, L.A., SABRI, M.A., IBRAHIM, T.H., KHAMIS, M.I., HAMDAN, N.M., AL-ASHEH, S., ALREFAI, M. and FERNANDEZ, C.

TITLE: Application of graphene nanoplatelets and graphene magnetite for the removal of emulsified oil from produced water.

YEAR: 2018

Publisher citation: CHACRA, L.A., SABRI, M.A., IBRAHIM, T.H., KHAMIS, M.I., HAMDAN, N.M., AL-ASHEH, S., ALREFAI, M. and FERNANDEZ, C. 2018. Application of graphene nanoplatelets and graphene magnetite for the removal of emulsified oil from produced water. Journal of environmental chemical engineering [online], 6(1), pages 3018-3033. Available from: https://doi.org/10.1016/j.jece.2018.04.060

OpenAIR citation: CHACRA, L.A., SABRI, M.A., IBRAHIM, T.H., KHAMIS, M.I., HAMDAN, N.M., AL-ASHEH, S., ALREFAI, M. and FERNANDEZ, C. 2018. Application of graphene nanoplatelets and graphene magnetite for the removal of emulsified oil from produced water. Journal of environmental chemical engineering, 6 (1), pages 3018-3033. Held on OpenAIR [online]. Available from: https://openair.rgu.ac.uk

Title: Application of graphene nanoplatelets and graphene magnetite for the removal of emulsified oil from produced water

Authors: Lamis Abou Chacra, Muhammad Ashraf Sabri, Taleb H. Ibrahim, Mustafa I. Khamis, Nasser M. Hamdan, Sameer Al-Asheh, Massa AlRefai, Carlos Fernandez

PII: S2213-3437(18)30236-7
DOI: https://doi.org/10.1016/j.jece.2018.04.060
Reference: JECE 2356

To appear in:

Received date: 7-1-2018
Revised date: 23-4-2018
Accepted date: 24-4-2018

Please cite this article as: Lamis Abou Chacra, Muhammad Ashraf Sabri, Taleb H.Ibrahim, Mustafa I.Khamis, Nasser M.Hamdan, Sameer Al-Asheh, Massa AlRefai, Carlos Fernandez, Application of graphene nanoplatelets and graphene magnetite for the removal of emulsified oil from produced water, Journal of Environmental Chemical Engineering https://doi.org/10.1016/j.jece.2018.04.060

Application of graphene nanoplatelets and graphene magnetite for the removal of emulsified oil from produced water

Lamis Abou Chacra[1], Muhammad Ashraf Sabri[1], Taleb H. Ibrahim[1,*], Mustafa I. Khamis[2], Nasser M. Hamdan[3] Sameer Al-Asheh[1], Massa AlRefai[1], Carlos Fernandez[4]

American University of Sharjah

[1]Department of Chemical Engineering

[2]Department of Chemistry, Biology and Environmental Sciences

[3]Department of Physics

P.O. Box 26666 Sharjah, United Arab Emirates

[4]School of Pharmacy and Life Sciences, Robert Gordon University, Aberdeen, AB10 7GJ, United Kingdom

*Corresponding author, Tel.:+971 6 5152460; fax: +971 6 5152979

Email address: italeb@aus.ed

ABSTRACT

Graphene and its magnetite derivative were used as adsorbents for removal of emulsified oil from produced water. The experimental parameters for maximum emulsified oil removal efficiency and effective regeneration of these adsorbents were determined. The best parameters in terms of dosage, contact time, pH, salinity and temperature were 3.00 g/L, 60.0 minutes, 10.0, 1500 ppm and 25.0 ºC for graphene nanoplatelets, and 4.00 g/L, 30.0 minutes, 3.5, 1000 ppm and 25.0 ºC, for graphene magnetite, respectively. Packed column studies were carried out utilizing graphene magnetite as adsorbent for the removal of oil from produced water. The packed column operation was assessed using Thomas, Yan et al., Clark, Bohart and Adams and Yoon and Nelson models. Thomas model was found to best describe the column experimental data. The column was regenerated using n-Hexane and reused several times for produced water treatment with negligible decrease in its initial capacity.

Keywords: adsorption; equilibrium isotherms; graphene magnetite; kinetic models; produced water; column studies

1. Introduction

Produced water is a major contributor to generation of wastewater streams, which is generated during the oil and gas extraction processes. It is estimated that around 3–9 barrels of water are produced per barrel of oil production by oil and gas industries[1]. Produced water contains many organic and inorganic materials; however, its chemical and physical characteristics vary depending on geographic location of the oil reservoir, existence of the reservoirs, nature of hydrocarbons produced, operating conditions and the added chemicals. Although the composition of the produced water can fluctuate according to different sources, they have common constituents analogous to the composition of oil/gas production [1-3].

Produced water is usually discharged to oceans and lakes without proper treatment and as such invokes serious environmental concerns. One of these concerns is the contamination of water body by oil which is hazardous to human and marine lives. Adverse negative effects on health have been reported related to the water contamination with oil and organic compounds. It is therefore necessary to treat produced water before it being discharged to the environment by the oil and gas companies [1-3].

Several methods have been applied to remove oil from produced water including hydrocyclones and membrane separation technologies [4-8]. Although both methods have been shown to be efficient, each of them has its drawbacks. Hydrocyclones are known to be widely used to treat produced water; however, its major disadvantage is the production of large slurry of solid waste. The difficulties of membrane are due to its scaling and fouling of the membrane as well as it requires extensive pretreatment. It is reported that the selection of appropriate technology

for produced water treatment depends on the influent and effluent water qualities, the waste generated as well as the overall cost [1, 9, 10].

Adsorption is another commonly used technique to remove oil from produced water. Activated carbon is one of the known and most promising adsorbent that is commonly used for the removal of a wide variety of organic compounds including oil. United States Environmental Protection Agency (USEPA) approved the use of activated carbon in adsorption applications as one of the best available technologies for the removal of organic compounds from air and water treatment processes. Since oil is mainly composed of organic compounds, activated carbon materials could be considered a suitable adsorbent for its removal [7,8]. Okiel et al. [11] conducted a study to remove emulsified oil from produced water using three different adsorbents, powdered activated carbon, deposited carbon, and bentonite. The adsorbents showed good oil removal efficiency in the range between 20 and 90 %. Adsorbents from biological origin have also been considered for this regard [12-15]. For example, eggshells was used as adsorbent for oil removal from water contaminated with oil (none emulsified) with 100% oil removal efficiency when using adsorption dosage of 1.8 g/L [12]. Banana peels was also proved to remove100% oil using 267 mg/L of the adsorbent at a contact time of 35 minutes [13].

Graphene is an emerging adsorbent to treat various pollutants, and could be an alternative to many other adsorbents. The special characteristics of this material make it an excellent candidate for different applications including electronics, energy storage, sensors, quantum dots and water treatment uses; as it has high mobility, high thermal conductivity, and admirable electronic and mechanical properties [16]. It has been applied successfully for the removal of metal ions and

organic contaminants from wastewater. When compared to zeolites, clay minerals, and other carbon materials, graphene showed higher adsorption capacity and better recycling capability for the removal of heavy metal ions [17, 18]. Graphene nanosheets are considered an excellent adsorbent for the treatment of wastewater produced from mining, dying and pesticides industries [19]. Graphene and graphene based materials were also used as adsorbents for different pollutants present in water including Methylene blue, Endosulfan, Saphranin T and Tetracycline [20]; the maximum adsorption capacity of these pollutants by such adsorbents were considered relatively high [20].

The objective of this work is to investigate the effectiveness of graphene nanoplatelets and its magnetite derivatives for the removal of emulsified oil from produced water and to determine the best conditions for the treatment process. Other related aspects will be also studied including sorption kinetics, sorption isotherms and graphene regeneration efficiency.

To the best of our knowledge, we present for the first time the applicability of graphene nanoplatelets and graphene magnetite for the removal of emulsified oil from produced water.

2. Materials and methods

2.1 Materials

Surfactant (ENDCOR OCC9783), heavy crude oil (having API < 22.3º), Industrial graphene nanoplatelets (GRAFEN®-iGP2, purity 99%), and n-Hexane (purity > 95%) were obtained from General Electric UAE, ADNOC UAE, Grafen Chemical Industries (Turkey) and J.T. Baker (Netherlands), respectively. Analytical grade chemicals were used, unless otherwise specified. 1.0 M sodium hydroxide and 1.0

M hydrochloric acid were used for pH adjustments. Salinity was adjusted using 1.0 M sodium hydroxide solution. GRAFEN®-iGP2 has diameter, thickness, density and surface area of 5-10 μm, 5 – 8 nm, 0.05 g/cm^3 and 120 -150 m^2/g, respectively. The graphene was cleaned with doubled distilled water and then washed with hexane and finally, dried in a vacuum oven prior to its use.

2.1 Instrumentations

The following instruments were used to perform the experimental part of this study: a temperature controlled shaker (Edmund Buhler, Germany) at 150 rpm, centrifuge (HERMLE Labortechnik GmbH, Germany) at 4000 rpm, Orion 201A+ basic pH meter (Thermo Electron Corporation, USA), and Cary 50 Conc (Varian, Australia) for UV-Visible measurements. Syringe filters (45 μm, PTFE Membrane, Chrom Tech, Germany) were also used. Characterization of adsorbents, before and after adsorption of oil, was carried out using several complementary techniques. Scanning electron microscopy (SEM) (TESCAN VEGA.3-LMU, USA), Z-potential measurements were conducted on Anton Paar Litesizer 500 (Austria), x-ray diffraction measurements (XRD) were performed using a Bruker D8 ADVANCE system with a Cu tube and a linear detector (LYNXEYE XE). The measurements were performed with a step size of 0.03°, 2θ range of 5° to 80°, and time per step of 2 s. Raman spectrum was performed using Rainshaw Raman InVia Microscope with laser excitation of 514 nm. The scan was performed for 600 s using a laser power of 0.5 W. XRD and Raman experiments were done at the Advanced Materials Research Laboratory at the University of Sharjah (UAE). Infrared spectra were recorded using Fourier transform infrared spectrometer (PerkinElmer, USA).

2.2 Preparation and stability of emulsion

Stable emulsion, to mimic industrial produced water, was prepared using 6:4 v/v ratio of surfactant to deionized water. Surfactant and deionized water were added in required quantities and stirred for homogeneity.

2.3 Preparation of graphene magnetite

Graphene magnetite was prepared as described elsewhere [21]with modification. Briefly, graphene (G) was placed in 100 mL aqueous solution, while Fe_3O_4 was prepared by adding Fe^{2+} ($FeSO_4$) :Fe^{3+} ($FeCl_3$) in a ratio1:2 by mass to another 100 mL aqueous solution sonicated by ultrasound for 10 minutes, and then 2-3 drops of concentrated HCl (6M) was added to ensure acidity of the solution. The Fe_3O_4 solution was added to the aqueous graphene solution, in ratio of graphene: Fe_3O_4 of 3:2, and then sonicated for 10 minutes for the purpose of homogeneity. Concentrated ammonia (15 M) was added to the solution to achieve a pH between 11 and 12. The solution was kept in a shaker hot bath at 50 ^oC for an hour. At this point, the solution was separated and the graphene magnetite (GM) precipitated. The solution was left for 1-2 days to digest and then the water-ammonia solution was filtered. The GM particles were washed with deionized water three times to ensure removal of any remaining water-ammonia on the surface. The GM particles were dried initially for two days at 60^oC in an oven and then finally dried in a vacuum oven at 60^oC for 3 hours.

2.4 Sorption tests

Batch tests as well as packed column adsorption modes were carried out. In all cases, a pre-specified emulsified oil concentration was prepared using surfactant: water ratio of 6:4. The salinity and pH of the sample was adjusted using either 1.0 M NaCl solution or 1.0 M NaOH solution.

In batch bench-scale experiments, known volume of emulsified oil was added into a flask and the known amount of adsorbent was added. The best results were achieved by varying the following parameters: adsorbent dosage (1-7 g/L), contact time (0-120 min), salinity (0-2000 ppm), pH (2-12) and temperature (25-50^{o}C). Upon achieving equilibrium, or a prescribed time for the case of studying kinetics of adsorption, the suspension was filtered using 0.45 μm syringe filters and known volume of filtrate was stirred with n-Hexane (3 times) for oil extraction from the samples. UV-Vis Spectroscopy, at a wavelength of 245nm was used to quantify the oil content [18]. The effect of experimental parameters was optimized for oil removal using G and GM.

In packed column mode, the effect of column height and flow rate was studied at the best conditions of pH, temperature and salinity as deduced from batch bench scale studies. The GM particles (0.3g – 0.6 g) were packed into a glass column (1 cm in diameter and bed depth 0.3 – 0.6 cm). Glass wool was placed at the bottom and top of the GM bed to ensure even distribution of solution and prevent particle floating. The produced water was fed to the bed and at regular time intervals samples were collected, filtered and quantified for the remaining oil content.

2.5 Sorption isotherms analyses

The applicability of different equilibrium isotherm models, including Temkin, Langmuir and Freundlich isotherm models, were assessed for the adsorption equilibrium isotherms data collected in this study for the different sorbate-sorbent systems. These models are described by equation 1A, 2A, and 3A, respectively, while 1B, 2B, and 3B represents the linearized forms of these isotherms, respectively.

$$q_e = B \ln[K_T C_e] \quad (1A)$$

$$q_e = B \ln K_T + B \text{ They } \ln C_e \quad (1B)$$

$$q_e = \frac{q_m K' C_e}{[1+K' C_e]} \quad (2A)$$

$$\frac{C_e}{q_e} = \frac{1}{K' q_m} + \frac{C_e}{q_m} \quad (2B)$$

$$q_e = k_f C_e^n \quad (3A)$$

$$\ln q_e = \ln k_f + n \ln C_e \quad (3B)$$

where q_e, C_e, q_m and k_f represents amount of oil being adsorbed at equilibrium per gram of adsorbent (mg/g), equilibrium concentration (mg/L), maximum adsorption capacity (mg/g) and Freundlich capacity parameter ($mg^{(1-1/n)}L^{1/n}/g$), respectively; K' and n are adsorption constants for Langmuir and Frendulich isotherms, related to energy of adsorption and adsorption intensity, respectively; K_T and B are Temkin sorption constants.

2.6 Thermodynamics

It is important to understand the thermodynamic nature of the adsorption process, which is achieved by calculating thermodynamic parameters such as Gibbs free energy ($\Delta G'$), enthalpy ($\Delta H'$) and entropy($\Delta S'$). Due to the nature and complexity

of the oil matrix under study, the average molar mass of the oil content was used to determine the equilibrium constant. Hence Sip's equation [22-25], was used to estimate the equilibrium constant as function of temperature. The Following equations are used to calculate these parameters for the considered sorbate-sorbent systems [22-25].

$$\Delta G' = -RTlnK_{eq} \quad (4)$$

$$K_{eq} = e^{-\Delta G'/\mathrm{RT}} \quad (5)$$

$$K_{eq} = K_{ad}^{-1} \quad (6)$$

$$Q_e = \frac{Q^T}{K_{ad}} C_e^N \quad (7)$$

$$lnK_{eq} = -\frac{\Delta H'}{RT} + \frac{\Delta S'}{R} \quad (8)$$

$$\Delta G' = \Delta H' - T\Delta S' \quad (9)$$

where, $\Delta G'$, $\Delta S'$ and $\Delta H'$are the apparent changes in Gibbs free energy (J/mol), entropy (J/mol.K) and enthalpy (J/mol) of adsorption, respectively. R, T and K_{eq} represent ideal gas constant (8.314J/mol.K), temperature (K) and apparent equilibrium constant. K_{eq} is found using equation (6). C_e, Q_e, and Q^T are the concentration of adsorbate in solution at equilibrium (mg/L), theoretical amount of oil being adsorbed at equilibrium per gram of adsorbent (mg/g) and theoretical maximum adsorption capacity (mg/g), respectively. K_{ad} and N are the fitting parameter. Plotting $\ln K_{eq}$ versus 1/T yields a straight line with $-\Delta H'/R$ as the slope from which the change in enthalpy can be calculated. $\Delta G'$ can be obtained from equation (4), hence using equation 6-7, $\Delta S'$ can be readily obtained. Determination of such parameters helps in deciding the endothermic or exothermic nature of the sorption process as well as whether the adsorption process of physisorption or chemisorption.

2.7 Sorption kinetics

Sorption kinetics provides an overview of the reaction path followed and the time required to attain equilibrium. Thus, sorption kinetics analysis is an important issue for understanding the extent of adsorbate uptake by the adsorbent; it helps in determining the mechanisms of the adsorption process itself [26, 27]. The commonly used models in this regard are the linearized forms of Lagergren model (pseudo first order kinetic model) and pseudo second order kinetic model; these are given by equations 10 and 11, respectively.

$$ln(q_e - q_t) = -k_I t + lnq_e \quad (10)$$

$$\frac{t}{q_t} = \frac{t}{q_e} + \frac{1}{K_{II} q_e^2} \quad (11)$$

Where q_t, k_I, k_{II} represent instantaneous adsorbate amount (mg/g), pseudo first order rate constant (1/min) and pseudo second order rate constant (g/mg.min), respectively.

3. Results and Discussions

3.1 Characterization of graphene and graphene magnetite

Figure 1 represents the SEM images for G and GM before and after adsorption. These images enable explaining the mechanism of the oil adsorption on the adsorbent's surface. Figures 1A and 1C, show the cavities and voids present on the surfaces of G and GM, respectively, while Figures 1B and 1D reflect the disappearance of these voids due to occupancy by the sorbate oil which results in changes of the surface of G and GM after adsorption.

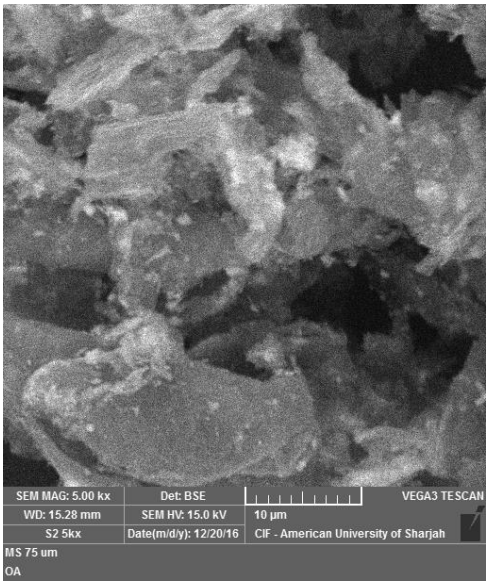

1A

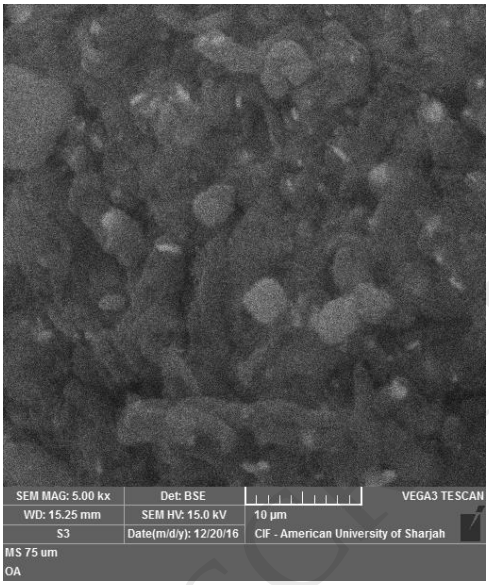

1B

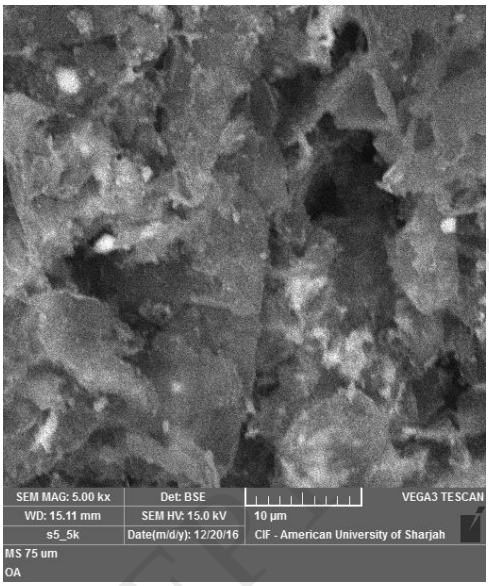

1C

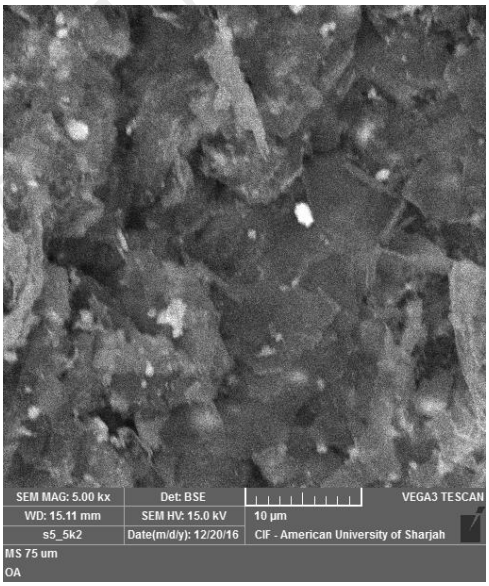

1D

Figure 1: SEM images of Graphene (G) before (1A) and after (1B) adsorption and Graphene magnetite (GM) before (1C) and after (1D) adsorption.

Figure 2 (a) shows the x-ray diffration pattern (XRD) of G, while figure 2 (b) shows the XRD pattern of GM. The XRD patterns confirm the structure of graphene nano particles in both samples. The pattern of GM sample shows the coexistance of

graphene and magnetite phases in the sample. Diffration peaks of garaphene are marked with (G) while those of magnetite are marked with (M) [28, 29]. Figure 3 shows the Raman spectra of G and GM samples. The spectrum of each sample shows the excepeted Raman structure of graphene nano partcles (or multilayers). The signiture of magnetite in GM was very week and shwon in figure 3 (c) [30-32].

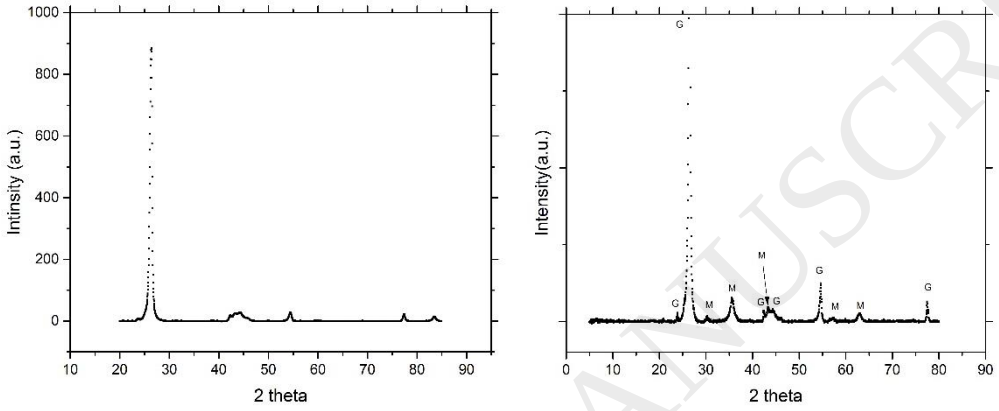

(a) (b)

Figure 2: (a) XRD pattern of graphene (G); (b) XRD pattern of graphene magnetite (GM). Peaks of graphene nano particles are marked with G, while peaks of magnetite are marked with M.

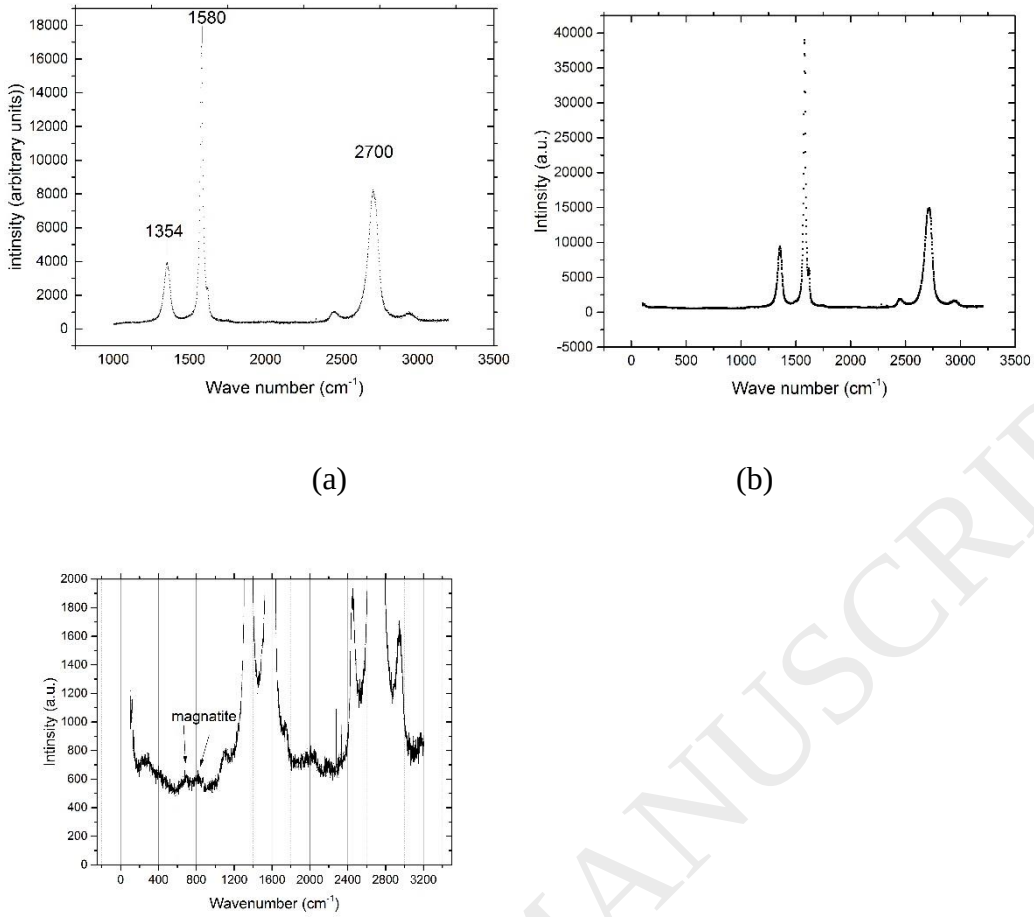

Figure 3: Raman Spectra of (a) pure graphene nano particles (G) showing the D band at 1354 cm^{-1}, the G band at 1580 cm^{-1} and the 2D (G') band at 2700 cm^{-1}; (b) the Raman spectrum for graphene magnetite GM sample basically showing the strure of graphene nano particles; and (C) enlargement of spectrum (b) showing the low peak of mgnetite at about 675 cm^{-1}.

Figure 4 displays the FTIR spectra of G and GM before and after emulsified oil adsorption. Inspection of this figure reveals that upon magnetization of graphene, new peak appears a ca 600 cm^{-1}. This peak is attributed to Fe-O stretching [33]. Furthermore, additional peaks were observed in G and GM spectra after batch adsorption of emulsified oil. In particular, new peaks appear in the range of 3500-

3800 cm^{-1}. Furthermore, the range 1000-1500 cm^{-1}, showed additional peaks indicating the presence of emulsified oil on these surfaces.

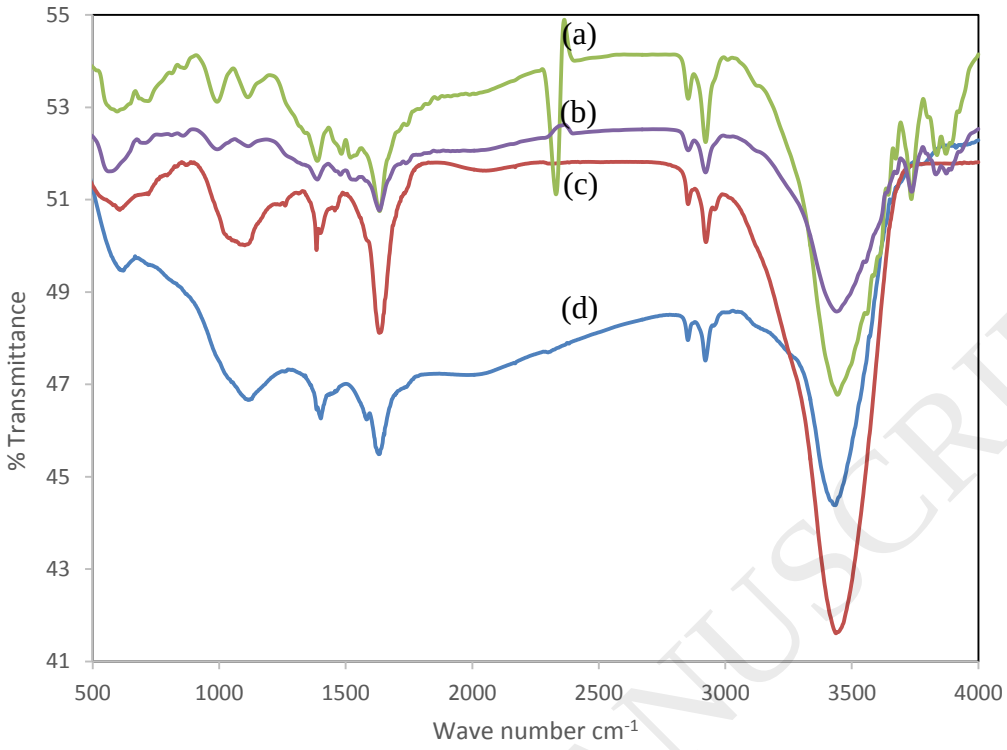

Figure 4: FTIR spectra of (a) G and (b) GM after oil adsorption (c) G and (d) GM before oil adsorption

The zeta potential of graphene and graphene magnetite are presented in figure 5 Inspection of this figure reveals that the zeta potential of graphene and its magnetite derivative is pH dependent. The point of zero charge (PZC) for graphene occurs at pH 2.2 while that of graphene magnetite occurs at pH 3.2. This indicate that at pH < 2, both surfaces are positively charged while at pH > 3.5, both surfaces are negatively charged. These results are used to explain the affinity of these adsorbents towards emulsified oil removal from produced water as function of pH.

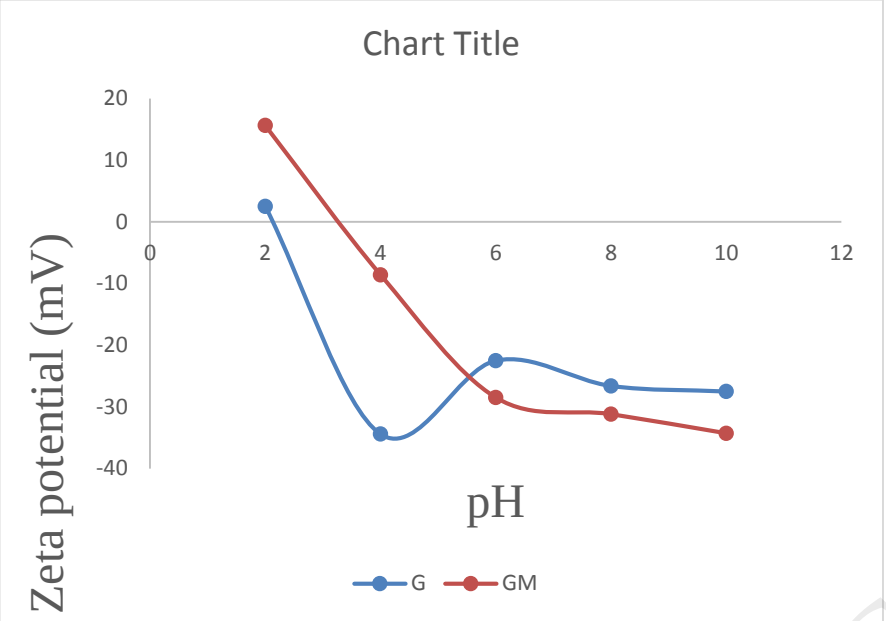

Fig. 5: Zeta potential of graphene (G) (blue) and graphene magnetite (GM) (red) at different pH values.

3.2 Effect of adsorbent dosage

Figure 6 shows the percent removal of emulsified oil by G and GM as a function of adsorbent dosage in the range of 1.0 – 6.0 g/L. At low dosages, the removal efficiency increased with the adsorbent dosage. The removal efficiency reached constant levels at dosages greater than 3.0 g/Land 4.0 g/L with maximum removal efficiency of 70.0 % and 49.6 % for G and GM, respectively. This could be due to the saturation of the adsorbent with the sorbate oil where all surface sites become occupied by the oil or adsorption is thermodynamically limited with no further driving forces under the specified conditions. Thus, the optimum adsorbent dosage was chosen to be 3.0 g/L and 4.0 g/L of G and GM, respectively.

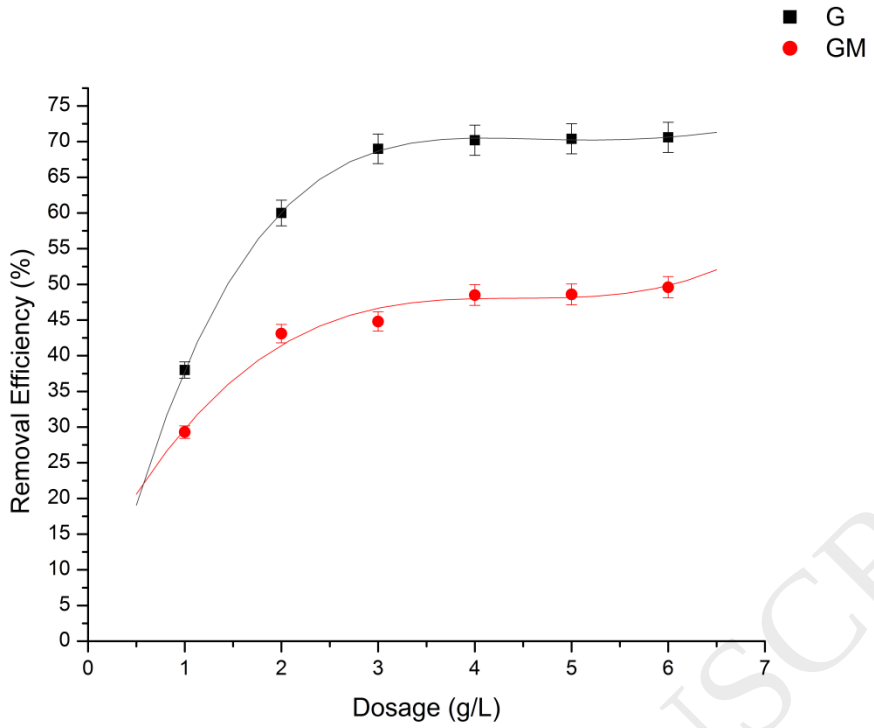

Figure 6: Effect of adsorbent dosage on the removal efficiency of emulsified oil by respective adsorbent. Initial oil concentration: 200 ppm; initial pH: 6.5 for GM and 7.98 for G; temperature 25^{o}C;contact time: 120 minutes; shaker speed: 150 rpm.

3.3 Effect of contact time

Figure 7 shows the percent removal efficiency of oil by G and GM as a function of contact time. Initially, the removal efficiency of emulsified oil increased rapidly with increasing the contact time. This is expected, as adsorption is normally a fast process. This would also indicate the spontaneous nature of the considered adsorption system due to the presence of available surface sites on the adsorbents, which with time become saturated with emulsified oil. Based on these results, the optimum time for removal of emulsified oil is 30 min for both adsorbents.

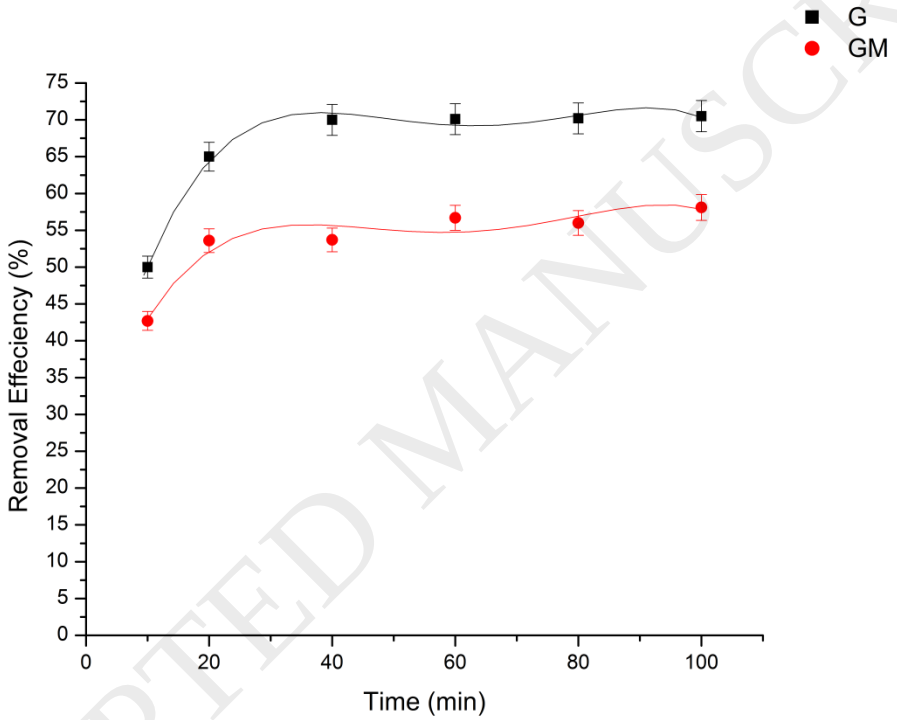

Figure 7: Effect of contact time on the removal efficiency of emulsified oil by G and GM adsorbents. Initial oil concentration: 200 ppm; initial pH: 6.5 (GM) 7.98 (G); temperature: 25^{o}C; shaker speed: 150rpm:dosage: 3 g/L (G) and 4 g/L (GM).

3.4 Effect of initial pH

Solution pH is an important parameter for any sorption system, and should be determined. The results for the percent removal of emulsified oil by G and GM as a function of pH, covering acidic and basic ranges, are shown in Figure 8. The figure shows that the removal efficiency increases with pH reaching 75.0% removal at pH of 10.0 for the case of G, while the maximum removal efficiency of emulsified oil in case of GM reached a level of 68.5% at a pH of 3.55. The different behavior of the two adsorbents in response to pH could be attributed to the nature of the surface of GM, as it is prepared from basic medium of G. The addition of iron particles to the GM might have significant influence on the removal efficiency. Furthermore, the higher efficiencies could be attributed to the instability of oil and related ions in aqueous medium. Based on these results, the optimum pH of 10.0 and 3.5 were chosen for G and GM, respectively.

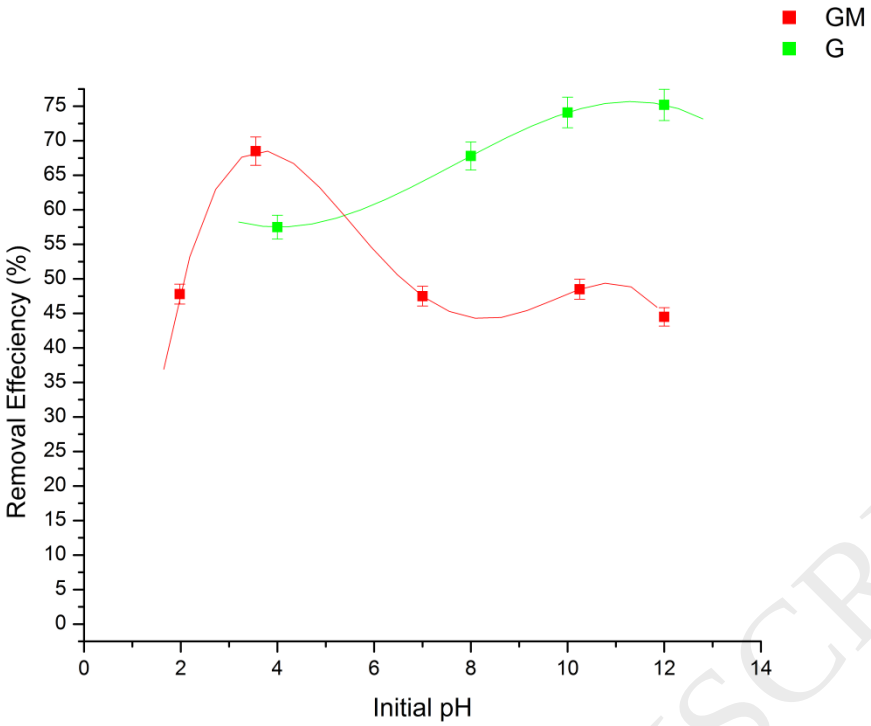

Figure 8: Effect of initial pH on the removal efficiency of emulsified oil by G and GM adsorbents. Initial oil concentration: 200 ppm; temperature: 25^{o}C; shaker speed: 150 rpm;sorbent dosage: 3g/L (G) and 4g/L (GM); contact time: 60 min (G) and 30 min (GM).

3.5 Effect of salinity

Figure 9 shows the effect of salinity on the percent removal of emulsified oil by G and GM. The percentage removal efficiency of the oil by both adsorbents showed almost same trends and it seems that removal efficiency slightly increases with increasing salinity up to1500 ppm. This increase could be due to the instability of emulsified oil in the aqueous medium as a result of higher affinity of NaCl ions towards water [12, 27]. Only very slight decrease in removal efficiency is noticed for salinity above 1500 ppm that can be because some adsorption sites might be blocked by saline ions and thus lowering the effective number of sites for emulsified oil adsorption.

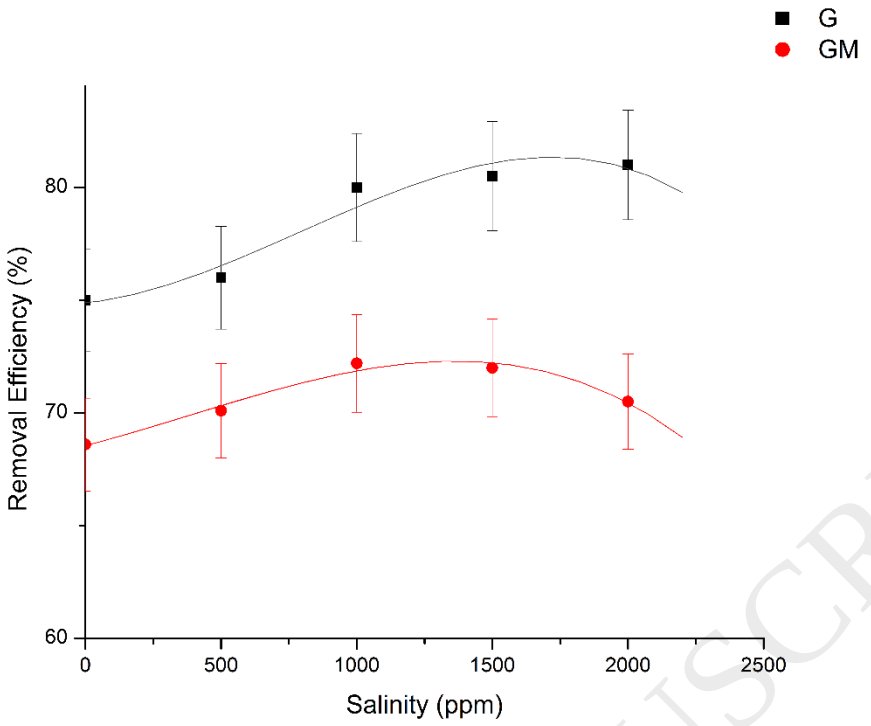

Figure 9: Effect of salinity on the removal efficiency of emulsified oil by the adsorbents G and GM. Initial oil concentration: 200 ppm; temperature: 25^{o}C; shakerspeed: 150 rpm;adsorbent dosage: 3 g/L (G) and 4 g/L (GM); contact time: 60 min (G), 30 min (GM); pH: 10 (G), 3.92 (GM)

3.6 Effect of temperature

The results for effect of temperature on the removal efficiency of emulsified oil using G and GM are shown in Figure 10. The experimental parameters were set at optimum values as deduced from the previous results. The removal efficiency of emulsified oil by graphene is highly affected by temperature while this effect is not pronounced when using the GM adsorbent. The percentage removal, in the case of graphene, decreased from 80 percent to 60 percent when increasing the temperature from 25 to 40^{o}C, respectively. However, the percentage removal of oil using GM remained almost constant even at 50^{o}C; this would suggest the possibility of using GM at various temperatures without losing its adsorption capacity and properties.

Thus, a temperature of 25 ^{o}C would be an optimum for both adsorbents. The decrease in percentage removal of emulsified oil with temperature by G could be attributed to the nature of interactions of the adsorbate with the active sites on G and the exothermic nature of the adsorption of emulsified oil by G [18]. On the other hand, for the case of GM, the adsorption process seems to be endothermic (ΔH = 27.6 ±0.8 kJ/mol). This explains the slight increase in the removal efficiency at higher temperatures. However, this slight increase in removal efficiency is not significant and thus the optimum temperature in case of GM is also 25^{o}C. This change in the nature of reaction from exothermic (in case of G) to endothermic (in case of GM) could be attributed to different mode of interactions between the various constituents of the emulsified oil and iron oxides modified surface.

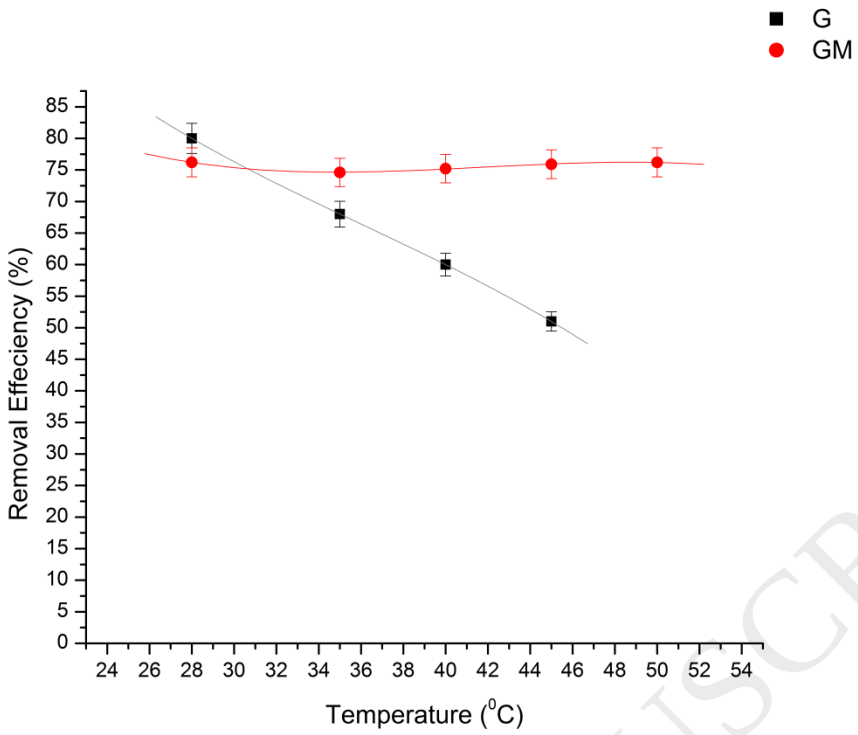

Figure 10: Effect of temperature on the removal efficiency of emulsified oil by G and GM adsorbents. Initial oil concentration: 200 ppm: shakerspeed: 150 rpm;adsorbent dosage: 3 g/L (G), 4 g/L (GM); contact time: 60 minutes (G), 30 minutes (GM); pH: 10 (G), 3.92 (GM);salinity: 1500 ppm (G), 1000 ppm (GM)

3.7 Effect of initial concentration of oil

The effect of initial emulsified oil concentration on percentage removal efficiency was studied at optimum conditions and the results are presented in Figure 11. It is clear that both adsorbents followed the same trend as the removal efficiency of both adsorbents declined appreciably by increasing the initial oil concentration. This is due to the fact that active sites gets occupied and saturated in case of higher

concentrations thus, decreasing the effective number of sites available for remaining oil to be adsorbed on adsorbent surface.

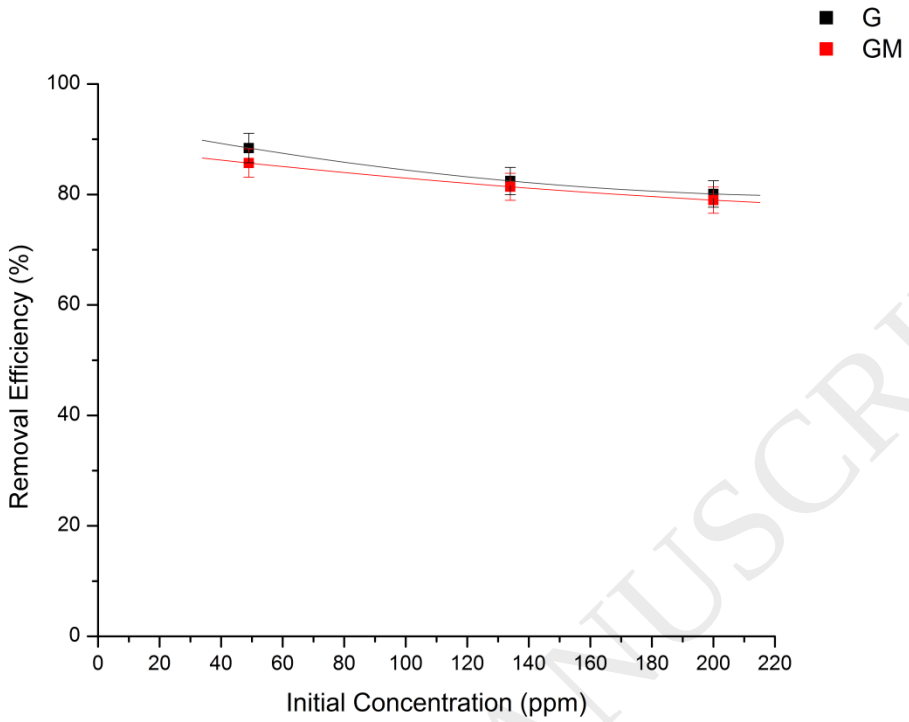

Figure 11: Effect of initial concentration on the removal efficiency of emulsified oil by G and GM adsorbents. Shaker speed: 150 rpm;temperature: 25^{o}C;adsorbent dosage: 3 g/L (G), 4 g/L (GM); contact time: 60 minutes (G), 30 minutes (GM); pH: 10 (G), 3.92 (GM);salinity: 1500 ppm (G), 1000 ppm (GM).

3.8 Adsorption isotherm

Experimental data for adsorption isotherms were collected for both adsorbent by varying the initial oil concentrations at the predetermined optimum conditions. The adsorption uptake at equilibrium, q_e, was calculated using the following equation

$$q_e = \frac{m_i - m_f}{m_g} \quad (12)$$

where m_i and m_f are the initial and final mass of oil in the solution in milligrams, and m_g is the mass (i.e. dosage) of the adsorbent in solution in grams.

The experimental adsorption data of the amount of oil adsorbed on G and GM were plotted as a function of final equilibrium concentration according to the different models previously described. Figures 12-14 show Langmuir, Freundlich and Temkin isotherms representations, respectively, for the two adsorbents. The parameters of these models were obtained from the slops and intercepts of the linear plots and summarized in Table 1. The relatively higher values of the R^2 for these adsorbents when using Freundlich model compared to that of Langmuir and Temkin models indicate better representation of the isotherm data by Freundlich. This indicates that the adsorption of emulsified oil on G and GM adsorbents is a function of the heterogeneity of the sample and the adsorption sites[34]. The value of the Freundlich constant n was less than one (Table 1) for both adsorbents indicating the favourable adsorption of emulsified oil onto each adsorbent. The Freundlich parameter, k_f, related to adsorption capacity is smaller for the case of GM than that of G. This could be due to the nature of the GM adsorbent that is characterized by iron particles impeded within the graphene framework. Although these magnetic particles renders the adsorbent to be easily recovered from solution by physical

magnetic field, it did not improve the adsorption capacity that could attribute to changes in the morphology and affinity of the surface toward oil removal.

Table 2 presents the emulsified oil adsorption capacities of different adsorbents. Graphite and carbon nanotube sponges showed higher sorption capacities for oil [18]. Organo-clay and modified bentonite clay used for emulsified oil treatment showed relatively lower adsorption capacities. In case of emulsified oil (oil with surfactant) treatment, the adsorption capacity of G and GM is significantly higher than the adsorption capacities of other adsorbents used for emulsified oil removal.

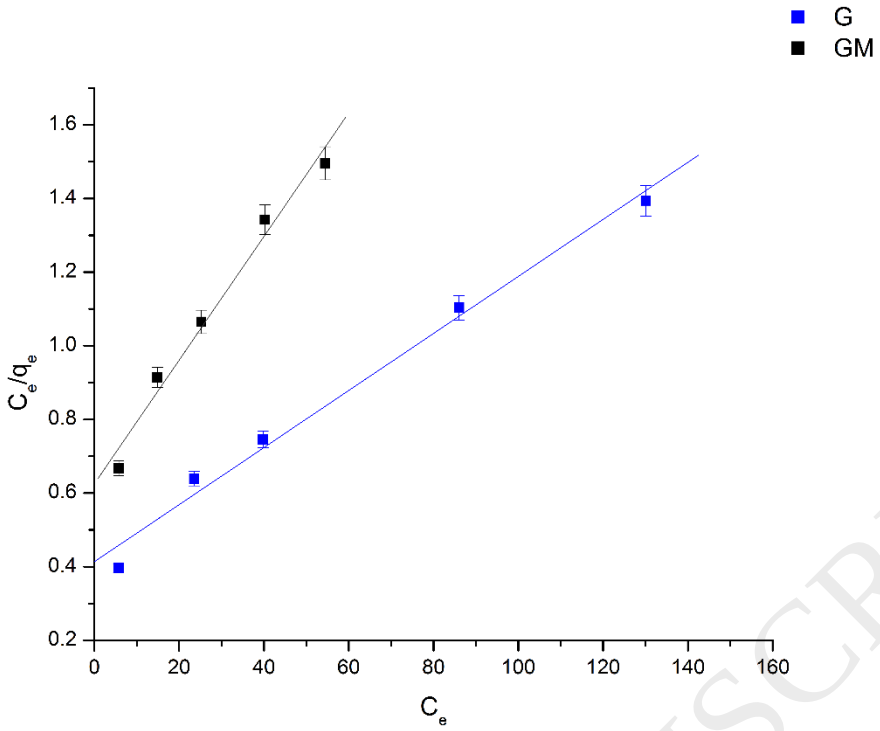

Figure 12: Langmuir adsorption isotherm for removal of emulsified oil by G and GM adsorbents. Shaker speed: 150 rpm;temperature: 25^{o}C;adsorbent dosage: 3 g/L (G), 4 g/L (GM); contact time: 60 minutes (G), 30 minutes (GM); pH: 10 (G), 3.92 (GM);salinity: 1500 ppm (G), 1000 ppm (GM).

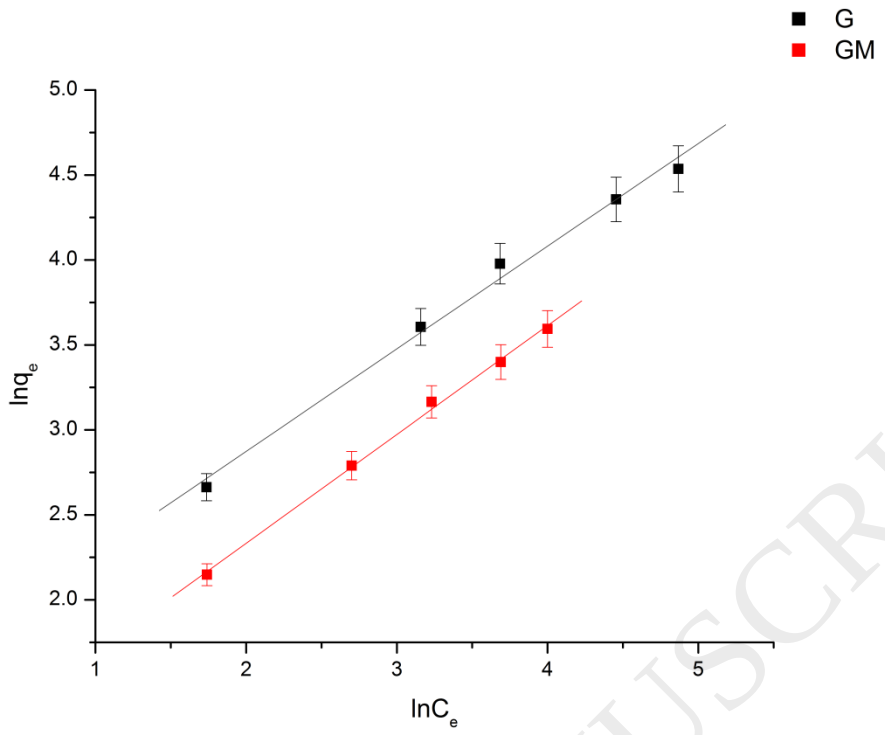

Figure 13: Freundlich adsorption isotherm for adsorption of emulsified oil. Parameters: shaking rate = 150 rpm, Temperature =25^{o}C, Dosage = 3 g/L (G), 4 g/L (GM), contact time = 60 minutes (G), 30 minutes (GM), pH = 10 (G), 3.92 (GM), Salinity = 1500 ppm (G), 1000 ppm (GM), temperature = 25^{o}C

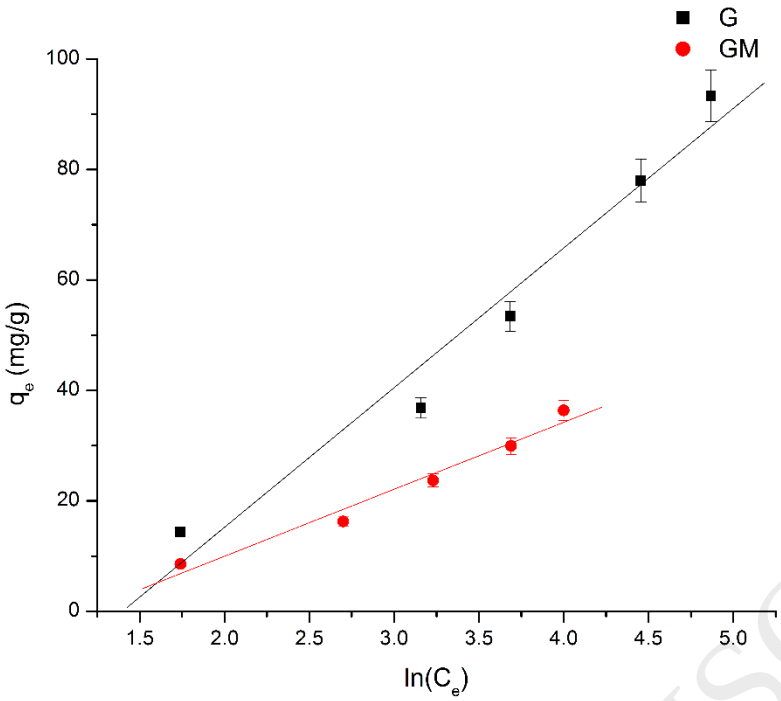

Figure 14: Temkin adsorption isotherm for adsorption of emulsified oil. Parameters: shaking rate = 150 rpm, Temperature =25°C, Dosage = 3 g/L (G), 4 g/L (GM), contact time = 60 minutes (G), 30 minutes (GM), pH = 10 (G), 3.92 (GM), Salinity = 1500 ppm (G), 1000 ppm (GM), temperature = 25°C

3.9 Kinetic models

Understanding the sorption kinetics of emulsified oil on the graphene nanoplatelets is an essential issue for scaling up the system. Various kinetic models are reported in the literature. However, the pseudo first order and pseudo second-order models were used for the experimental data of this work as they are simple, most suited and widely used models. Representations of the experimental data following these models are shown in figures 15 and 16 with corresponding parameters determined from these figures displayed in Table 3. The low values of R^2 for pseudo first order kinetics of 0.891 and 0.734 for the case of G and GM, respectively, indicates poor

representation of the data by the pseudo first order kinetic model. The higher R^2 values following pseudo-second order kinetics, 0.999 and 0.999 using G and GM, respectively, indicate excellent representation of the data by this model (Table 3). Kinetics data following the pseudo-second order model indicate intra-pore diffusion of the emulsified oil on the adsorbent. The maximum adsorption capacity, q_e, calculated by pseudo-second order model is comparable to the actual maximum adsorption capacity value with a percentage error of 1.10 % and 4.30 % in case of G and GM, respectively. The absolute relative error in the maximum adsorption capacity calculated from other models is very high as compared to q_e value measured experimentally (Table 3).

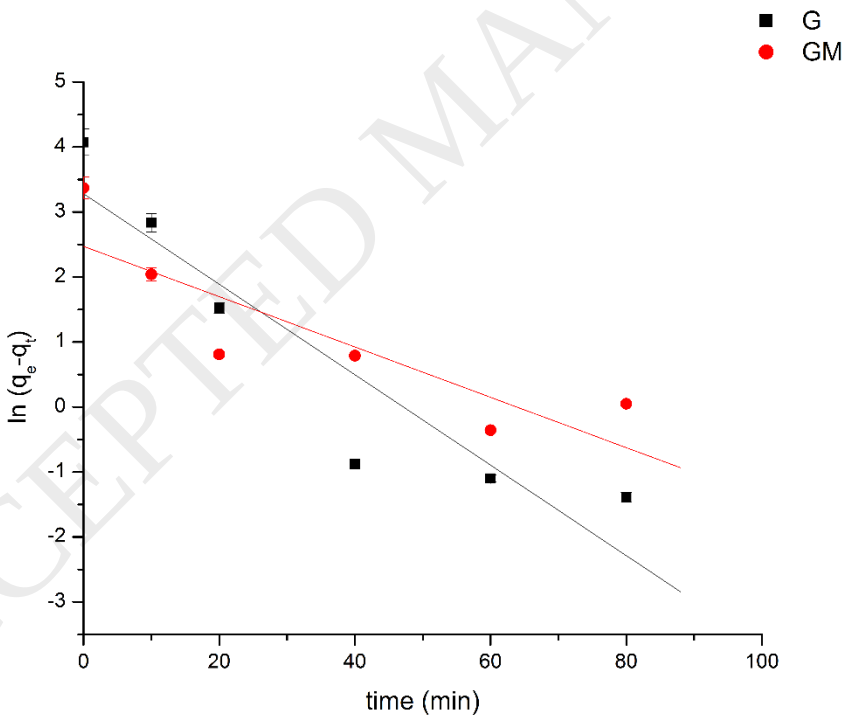

Figure 15: Pseudo first order kinetics for emulsified oil adsorption usinf G and GM adsorbents. Shaker speed: 150rpm;temperature: 25^{o}C;adsorbent dosage: 3 g/L (G), 4 g/L (GM), pH: 6.5 (GM), 7.98 (G).

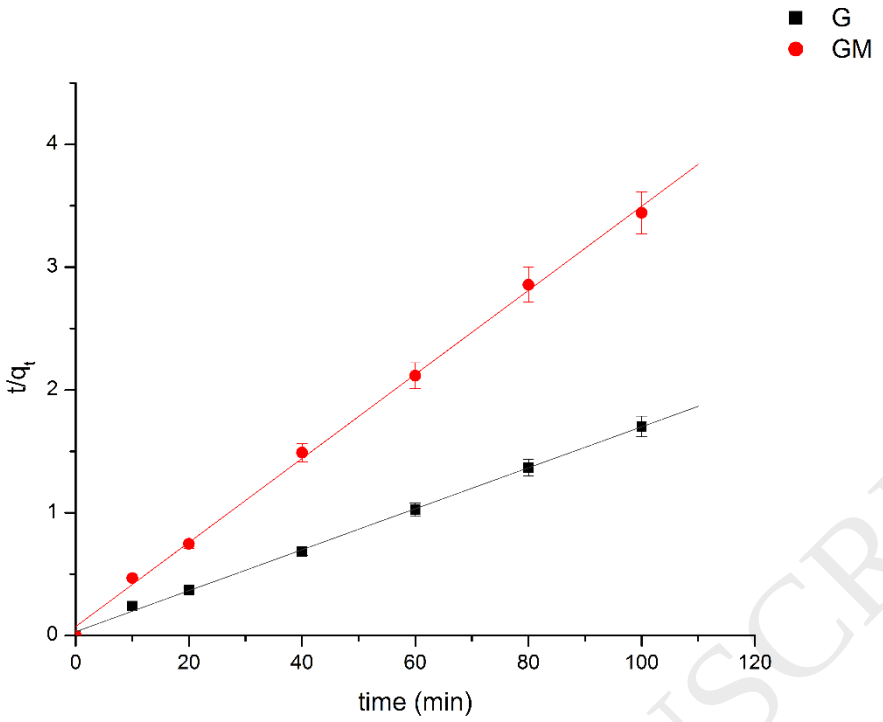

Figure 16: Pseudo second order kinetics for emulsified oil adsorption using G and GM adsorbents. Shaker speed: 150rpm;temperature: 25°C;adsorbent dosage: 3 g/L (G), 4 g/L (GM); pH: 6.5 (GM), 7.98 (G).

3.10 Thermodynamic parameters

Thermodynamic parameters for the sorption of emulsified oil on graphene magnetite nano-platelets were determined at the optimum experimental conditions as deduced from the previous results. The ΔH' value was determined from the slope of the linear plot of $\ln K_{eq}$ versus T^{-1} (Figure 17).

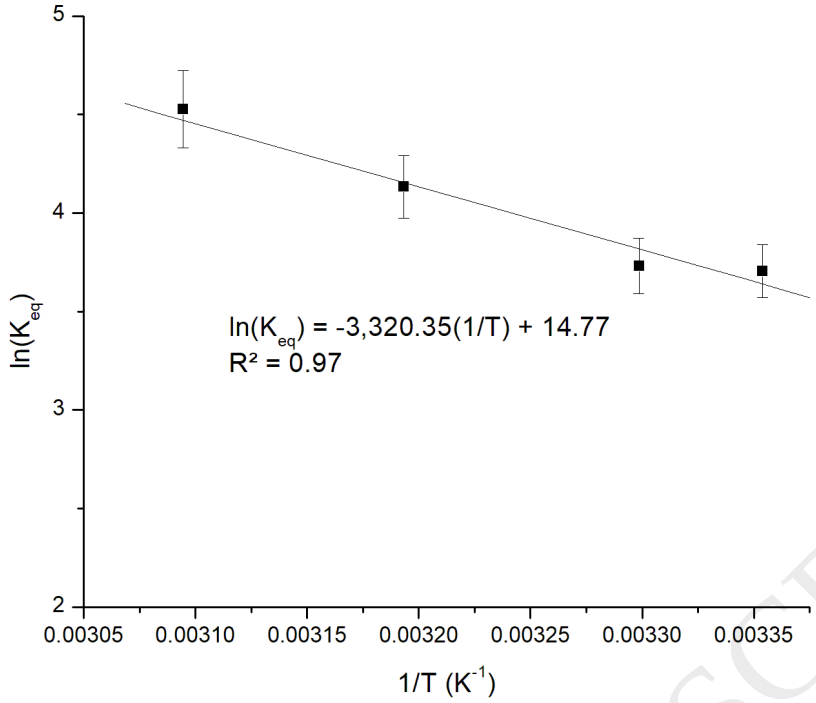

Figure 17: Thermodynamic study for emulsified oil adsorption on graphene magnetite

The values of n, K_{ad}, ΔG' and Q^T were estimated by regression analysis for the adsorption of oil on graphene magnetite at various temperatures are presented in Table 4. Table 5 displays the thermodynamic parameters as calculated using equations 4-8. The positive sign of enthalpy change of adsorption supports the conclusion of endothermic nature of the considered adsorption process using graphene magnetite. Typically for the physisorption processes, the range of the values for free energy (ΔG') is between −20.0 and zero kJ/mol whereas for the chemisorption processes the range of ΔG' is between −80.0 and −400 kJ/mol [35]. Because the values of (ΔG') for this study are within -20 to zero kJ/mol, it means the process is physisorption. The apparent change in Gibbs energy (ΔG') increases with the increase in the temperature, which means low feasibility of adsorption at higher temperatures. The negative sign of Gibbs free energy indicate the

spontaneous nature of the sorption process. The positive value of ΔH′ obtained indicates that the adsorption of oil onto graphene is endothermic in nature. Furthermore, the apparent change in entropy being positive means an increase in the randomness of the solid/solution boundary of the adsorption process [21, 36].

3.11 Packed-column operation

Prediction of breakthrough curve or concentration-time profile for effluent is necessary for the successful adsorption column design. In general, sorption mechanisms involves adsorption kinetics at surface or pores of adsorbent, resistances to film diffusion as well as intra-particle diffusion including both surface & pore diffusion and axial dispersions in liquid flow direction. The prediction of breakthrough curve or adsorption column design requires numerical rigorous approaches, in general. However, several mathematical models for concentration-time profile or breakthrough curve prediction have been reported in literature. The most common ones are 1) Thomas model, 2)Yan et al. model, 3) Clark model, and 4) Bohartand Adams model as presented in Eqs.13-16, respectively [37, 38]. The linearized forms of these models as shown in Figure 18 represented the experimental breakthrough data of this work using GM adsorbent.

$$\ln\left[\frac{C_o}{C_e}-1\right]=\frac{q_T M K_{TH}}{Q}-C_o K_{TH} t \quad (13)$$

$$\ln\left[\frac{C_e}{C_o-C_e}\right]=a\ln[V]-a\ln[b] \quad (14)$$

$$\ln\left[\left(\frac{C_o}{C_e}\right)^{n-1}-1\right]=\ln[A]-rt \quad (15)$$

$$\ln\left[\frac{C_o}{C_e}-1\right]=\frac{N_o Z K_{BA}}{U}-C_o K_{BA} t \quad (16)$$

where t, C_o, C_e, n are breakthrough time (min), influent oil concentration (mg/L), effluent oil concentration at time t (mg/L) and Freundlich isotherm parameter. K_{TH}, K_{BA} are rate constants for Thomas, and Bohar & Adams, respectively. a and b are Yan model parameters while A and r (1/min) represent model parameters for Clark equation.

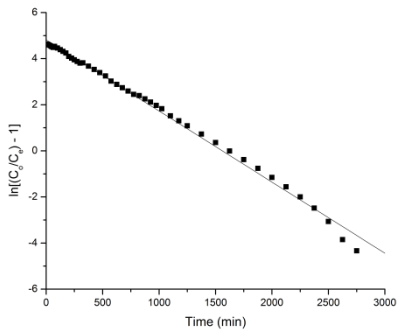

(A)

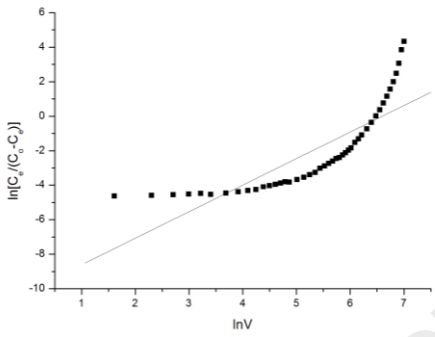

(B)

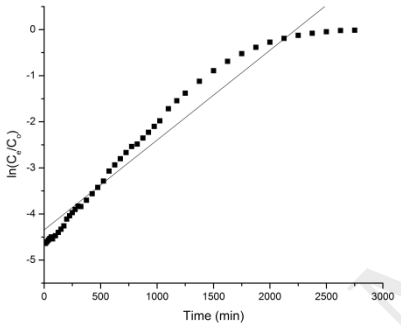

(C)

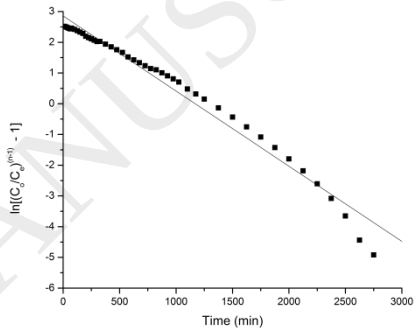

(D)

Figure 18: Linearized form of the break-through curve for emulsified oil adsorption on GM. Packed amount of adsorbent: 0.7 g;influent flow rate: 0.4 ml/min,;temperature: 25^{o}C; pH: 6.5;salinity: 1000 ppm;influent oil concentration: 200 ppm. (A) Thomas, (B) Yan et al., (C) Bohart & Adams, (D) Clark.

The regression coefficients of these linearized models along with the respective R^2 value have been calculated and are summarized in Table 6. As of R^2 value displayed in Table 6, it can be said that the adsorption of oil on GM in fixed bed column is

perfectly represented by Thomas model. Thomas model is most widely used model for column performance evaluation. The applicability of Thomas model to the fixed bed adsorption process suggests that the diffusion (internal and external) is not the limiting step in the process [39]. Table 7 shows that the effects of flow rates and column bed height on the k_{Th} and q_o as determined from Thomas adsorption model. It is apparent that an increase in column bed height decreases the k_{Th} and increases the q_o value. Furthermore, the values of k_{Th} increases and q_o decreases at higher flow rates. Thus, lower flowrates and higher bed heights would significantly increase the oil adsorption onto GM.

Effect of bed depth

The effect of bed depth on the column profile or breakthrough curve is shown in Figure 19. It is seen that increasing the bed height from 1.5 (0.45 g of packing) to 2 cm (0.6 g of packing) resulted in longer breakthrough time and service time of the column. The concentration-volume or concentration time profile follows Thomas model in the initial stages, however as the value of C_e/C_o goes above 0.6, the deviations increase which may be due to the buildup and interactions of oil adsorbed on the surface of the GM and the oil present in the produced water sample.

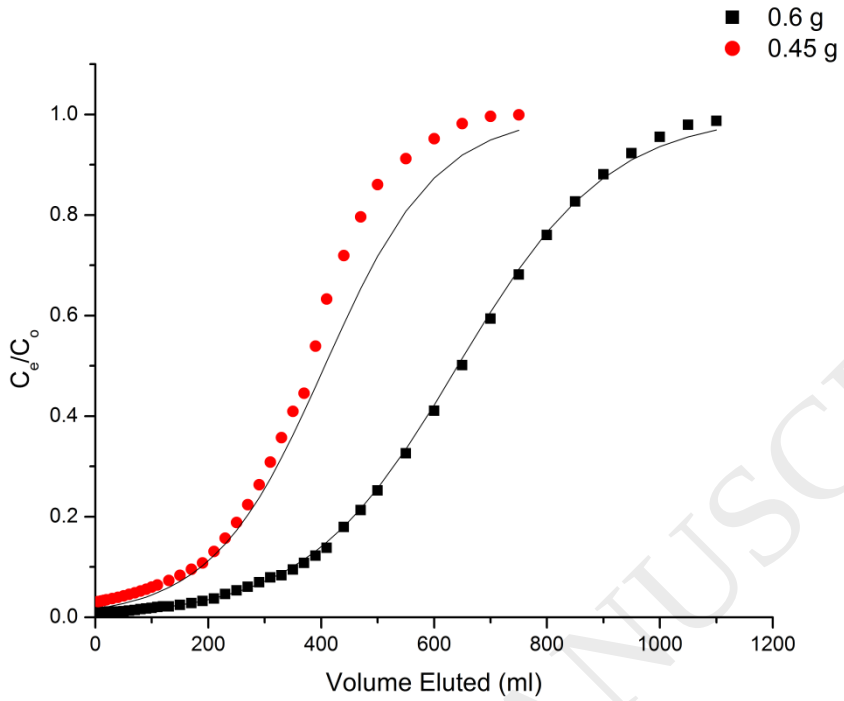

Figure 19: Effect of columnn depth on column performance. Amount of GM adsorbent: 0.6 g 2 cm bed depth and 0.45 g for 1.5 cm bed depth;Influent flow rate: 0.4 ml/min;temperature: 25^{o}C; pH: 6.5;salinity = 1000 ppm;influent oil concentration: 200 ppm.

Effect of flow rate

The effect of influent flow rate, while keeping bed height constant, on the breakthrough curve is shown in Figure 20. It is seen that increasing the flow rate from 0.4 mL/min to 0.8 mL/min resulted in a shorter breakthrough time and service time of the column. This effect can be attributed to less contact time between the adsorbent and the adsorbate resulting in less adsorption of oil molecules on GM. Again, the concentration-volume or concentration time profile follows Thomas model in the initial stages, however, as the value of C_e/C_o goes beyond0.6, the

deviations increases which could be due to the buildup and interactions of oil adsorbed on the surface of the GM and the oil present in the produced water sample. The clear shift in the shape of the curve with almost the same removal efficiencies when C_e/C_o (for flow rates of 0.4 and 0.8 mL/min) exceeded a value of 0.7 can be attributed to the fact that at same adsorbent loading, higher flow rate (0.8 mL/min) generates lower breakthrough curves and removal at corresponding eluted volumes. However, as the column starts saturating with oil, the oil adsorbed interacts with the oil in the produced water sample and helps in retaining of oil from produced water on to the GM surface, thus increasing the effective adsorption of oil on GM comparable to adsorption profile at 0.4 mL/min.

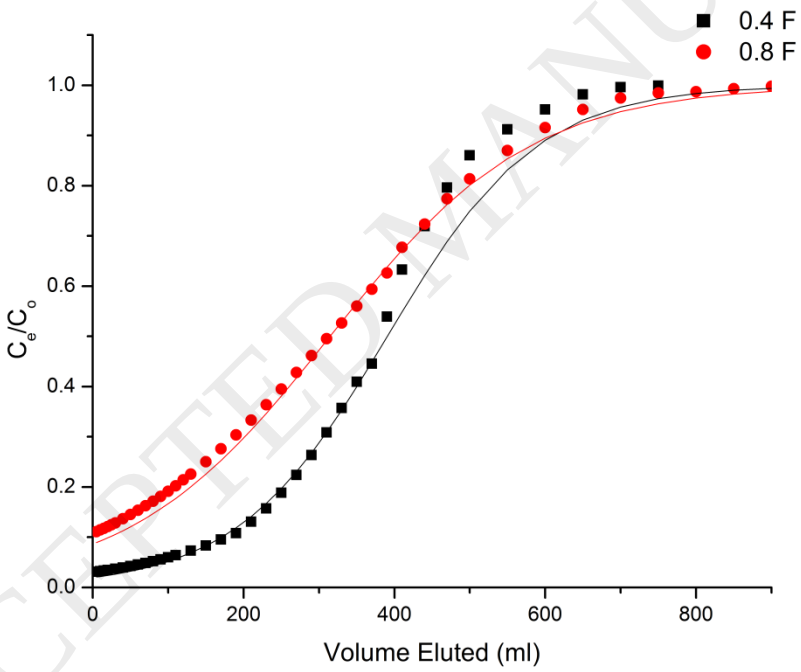

Figure 20: Effect of flow rate on column performance. Amount of adsorbent: 0.45 g of GM (bed depth of 1.5 cm);temperature: 25°C; pH: 6.5;salinity: 1000 ppm;influent oil concentration: 200 ppm.

3.12 Graphene Regeneration Study

Sorbent regeneration was considered using batch-bench scale tests. In this case, 40mL of emulsified oil (produced water sample, as described before) were transferred into Erlenmeyer flasks, optimum dosage of G and GM was then added in separate flasks and the conditions were fixed at optimum as previously determined. The removal efficiency was determined as discussed before. Afterwards, the system was filtered G and GM were dried and then mixed with n-Hexane to re-cover the oil adsorbed on these adsorbents. These regenerated adsorbents were used again in the similar fashion for further adsorption test. Two cycles of oil adsorption-desorption on G and GM, respectively, were carried out to evaluate the percentage efficiency of regeneration cycle. The percent removal efficiency showed a slight decrease over the two adsorption-regeneration cycles;- 4.10% (80.0 % to 75.9%) in the first cycle and - 3.50% (75.0 % to 71.5 %) in the second cycle, respectively, in case of G adsorbent. In case of GM, the decrease in percent removal efficiency over the two cycles was relatively lower, i.e. - 2.10 % and - 2.5% for first and second cycle, respectively. These results suggest that G and GM can be effectively regenerated and re-used without any significant compromise in their adsorption potentials.

Regeneration tests were also considered in the packed-bed operation. In this case, the column was packed with GM adsorbent (0.6 g, bed depth: 2 cm, flow rate: 0.4 mL/min) and the column efficiency was determined as discussed previously. After column saturation ($C_e/C_0 = 1$), the column was regenerated by backwash using n-Hexane at a flow rate of 0.2 mL/min to ensure enough contact time for oil to be transferred from GM surface to n-Hexane. After regeneration, the column was washed with water to ensure pH as that of the initial value. Adsorption-regeneration

cycles were performed twice in order to verify the efficiency of the process. The adsorption-desorption column study resulted in almost the same concentration-eluted volume (time) curves for all cases with maximum decrease in removal effectiveness of about 3.5 % at respective eluted volume calculations. Thus, this study supports the potential use of GM as adsorbent to be used in batch as well as packed-column operations. The only drawback of GM is its high tendency to pack. After elution of 1L of solution, the packing of GM was observed to be increased with effective volume decrease up to 0.2 mL, from the start of first experiment. Thus, intermittent air blows to ensure that GM does not pack enough to hinder the flow rate seems necessary.

3.13 Real Produced Water

Real produced water samples obtained from ADNOC Company were subjected to batch studies at the optimum parameters to study the adsorption results for G and GM. The initial oil concentration in produced water samples, percent removal efficiency of emulsified oil using G and GM adsorbents were determined to be 268 mg/L, 90.0% and 72.2 %, respectively. This supports the validity of work conditions considered in this work, the high efficiency of the G and GM for emulsified oil removal from produced water.

4. Conclusions

Batch and packed-column adsorption studies for emulsified oil adsorption from produced water were carried out using graphene and graphene magnetite. The optimum parameters were identified for the batch-bench scale adsorption tests and these were utilized in packed-column studies. The percentage removal efficiency of

emulsified oil at the optimum parameters exceeded 80 percent for graphene and 75 percent for graphene magnetite. The removal efficiency was identified to be enhanced by the increase in the salinity and the decrease in the initial emulsified oil concentrations. Oil adsorption by both adsorbents showed to fit Freundlich's isotherm and follow pseudo second order kinetics. The maximum adsorption capacities of graphene and graphene magnetite were found to be100 mg/g and 85 mg/g, respectively. In packed-column operation, Thomas model was identified to best fit the experimental data with q_o and K_{TH} to be 183.4 mg/g and 0.015 ml/mg.min, respectively. Two consecutive adsorption-regeneration cycles showed the possibility of these adsorbents to be used and regenerated successfully without major change in their efficiency in batch as well as in packed-column operation. In addition, graphene nanoplatelets and graphene magnetite were capable of treating a real sample of industrial produced water and showed 90.0 % and 72.2 % oil removal efficiency in batch studies, respectively.

Acknowledgments

This work was supported by American University of Sharjah UAE. The authors would like to thank Abu-Dhabi National Oil Company for providing the crude oil and General Electric for supplying the oil surfactant and Anton Paar Middle East Technical Center and BDH MIDDLE EAST LLC, Dubai, for their help in running the zeta potential measurements. We also acknowledge of the Advanced Materials Research Laboratory at the University of Sharjah, where the XRD and RAMAN measurements were performed. In addition, the authors would like to extend their appreciation to Mr. Thomas Job and Mr. Ziad Sara for their technical support.

References

[1] A. Fakhru'l-Razi, A. Pendashteh, L. C. Abdullah, D. R. A. Biak, S. S. Madaeni, and Z. Z. Abidin, "Review of technologies for oil and gas produced water treatment," Journal of Hazardous Materials, vol. 170, no. 2–3, (2009) 530-551.

[2] R. R. Reynolds, R. D. Kiker, "Produced water and associated issues a manual for the independent operator," South-Midcontinent Region, PTTC, vol 6, 2003.

[3] Z. Khatib and P. Verbeek, "Water to Value - Produced Water Management for Sustainable Field Development of Mature and Green Fields," Society of Petroleum Engineers, SPE International Conference on Health, Safety and Environment in Oil and Gas Exploration and Production, Kuala Lumpur, Malaysia, 2002.https://www.onepetro.org/conference-paper/SPE-73853-MS. (accessed 03.01.2017)

[4] P. McCormack, P. Jones, M. J. Hetheridge, and S. J. Rowland, "Produced water treatment technologiesAnalysis of oilfield produced waters and production chemicals by electrospray ionisation multi-stage mass spectrometry (ESI-MSn)," Water Research, vol. 35, no. 15, (2001) 3567-3578.

[5] J. E. Drewes, T. Y. Cath, P. Xu, J. Graydon, J. Veil, and S. Snyder, "An integrated framework for treatment and management of produced water," RPSEA Project, Golden, Colorado, http://www.rpsea.org/media/files/project/33e65b3c/EVNT-PR-07122-

12_2009_Integrated_Framework_Treatment_Management_Produced_Water-Drewes-4-14-09.pdf, 2009.(accessed 03.01.2017)

[6] S. Alzahrani and A. W. Mohammad, "Challenges and trends in membrane technology implementation for produced water treatment: A review," Journal of Water Process Engineering, vol. 4, (2014) 107-133.

[7] J. D. Arthur, B. G. Langhus, and C. Patel, "Technical summary of oil & gas produced water treatment technologies," ALL Consulting, LLC. South Cheyenne Ave., Tulsa, OK,http://www.all-llc.com/publicdownloads/ALLConsulting-WaterTreatmentOptionsReport.pdf. 2005, (accessed 03.01.2017).

[8] F. Bayati, J. Shayegan, and A. Noorjahan, "Treatment of oilfield produced water by dissolved air precipitation/solvent sublation," Journal of Petroleum Science and Engineering, vol. 80, no. 1, (2011) 26-31.

[9] T. Hayes and D. Arthur, "Overview of emerging produced water treatment technologies," in 11th Annual International Petroleum Environmental Conference, Albuquerque, NM, 2004

[10] E. T. Igunnu and G. Z. Chen, "Produced water treatment technologies," International Journal of Low-Carbon Technologies, vol 9, no. 3, (2014) 157-177.

[11] K. Okiel, M. El-Sayed, and M. Y. El-Kady, "Treatment of oil–water emulsions by adsorption onto activated carbon, bentonite and deposited carbon," Egyptian Journal of Petroleum, vol. 20, no. 2, (2011) 9-15

[12] I. Muhammad, U. El-Nafaty, S. Abdulsalam, and Y. Makarfi, "Removal of oil from oil produced water using eggshell," Civil and Environmental Research, vol. 2, no. 8, (2012) 52-63.

[13] U. El-Nafaty, I. Muhammad, and S. Abdulsalam, "Biosorption and kinetic studies on oil removal from produced water using banana peel," Civil and Environmental Research, vol. 3, no. 7, (2013) 125-136.

[14] T. H. Ibrahim, A. S. Gulistan, M. I. Khamis, H. Ahmed, and A. Aidan, "Produced water treatment using naturally abundant pomegranate peel," Desalination and Water Treatment, vol. 57, no. 15, (2016) 6693-6701.

[15] T. H. Ibrahim, M. A. Sabri, M. I. Khamis, Y. A. Elsayed, Z. Sara, and B. Hafez, "Produced water treatment using olive leaves," Desalination and Water Treatment, vol. 60, (2017) pp. 129-136.

[16] J.-G. Yu et al., "Graphene nanosheets as novel adsorbents in adsorption, preconcentration and removal of gases, organic compounds and metal ions," Science of the Total Environment, vol. 502, (2015) 70-79.

[17] M. Berger, "Nanotechnology water remediation with bulky graphene materials," http://www.nanowerk.com/spotlight/spotid=34951.php 2014 (accessed: 03.01.2017)

[18] L. Abou Chacra, "Treatment of produced water using graphene," Master of Science inChemical Engineering, Department of Chemical Engineering, American University of Sharjah, Sharjah, U.A.E., 2016.

[19] S. Chowdhury and R. Balasubramanian, "Recent advances in the use of graphene-family nanoadsorbents for removal of toxic pollutants from wastewater," Advances in Colloid and Interface Science, vol. 204, (2014) 35-56.

[20] X. Wang, B. Liu, Q. Lu, and Q. Qu, "Graphene-based materials: Fabrication and application for adsorption in analytical chemistry," Journal of Chromatography A, vol. 1362, (2014) 1-15.

[21] Ö. Kerkez-Kuyumcu, Ş. S. Bayazit, and M. A. Salam, "Antibiotic amoxicillin removal from aqueous solution using magnetically modified graphene nanoplatelets," Journal of Industrial and Engineering Chemistry, vol. 36, (2016) 198-205.

[22] Y. Liu and Y. Liu, "Biosorption isotherms, kinetics and thermodynamics", Separation and Purification Technology, vol. 61, (2008) 229-242

[23] E.C. Lima, M.A. Adebayo, F.M. Machado, "Chapter 3 - Kinetics and equillibrium modesl of adsorption" in carbon nanomaterials as adsorbetns for environmental and biological applications, C.P. Bergmann, F.M. Machado editors, Springer 2015, pp. 33-69. DOI: 10.1007/978-3-319-18875-1_3

[24] Y. Liu, "Is the free energy change of adsorption correctly calculated?", Jounal of chemical and engineering data, vol. 54, (2009), 1981-1985

[25] Y. Liu, H. Xu, "Equillibrium, thermodynamics and mechanism of Ni2+ biosorption by aerobic granules", Biochemical engineering journal, vol. 35, (2007) 174-182

[26] B. Saha and C. Orvig, "Biosorbents for hexavalent chromium elimination from industrial and municipal effluents," Coordination Chemistry Reviews, vol. 254, no. 23–24, (2010) 2959-2972.

[27] A. S. Gulistan, "Oil Removal From Produced Water Using Natural Materials," Master of Science in Chemical Engineering, Department of Chemical Engineering, American University of Sharjah, Sharjah U.A.E., 2014.

[28] M. Ara, K. Wadumesthrige, T. Meng, S. O. Salley, K. Y. Simon Ng, " Effect of microstructure and Sn/C ratio in SnO2–graphene nanocomposites for lithium-ion battery performance", RSC Adv. Vol. 4, (2014) 20540-20547

[29] G. Wang, J. Yang, J. Park, X. Gou, B. Wang, H. Liu, J. Y., "Facile Synthesis and Characterization of Graphene Nanosheet". J. Phys. Chem. Vol. 113, (2008) 8192-8195.

[30] M. Wall, "The Raman Spectroscopy of Graphene and the Determination of Layer Thichness", Application Note: 52252, (2011) 1-5.

[31] W. Wanga, S. Guob, I. Ruizc, M. Ozkanb, C. S. Ozkana, "Three Dimentional Graphene-CNTs Foam Architectures for Electrochemical Capacitors", ECS Trans. Vol 50, no. 43, (2013) 37-44.

[32] Y. Lin, C.Y. Yang, J. H. Liou, C. P. Yu, G.R. Lin, "Using graphene nano-particle embedded in photonic crystal fiber for evanescent wave modelocking of fiber laser", Optics Express, Vol. 21,no. 14, (2013) 16763-16776.

[33] J.W Jusin , M. Aziz, G.P. Sean, J. Jaafa, Preparation and Characterization of Graphene-based Magnetic Hybrid Nanocomposite", Malaysian J. of Analy. Sc., Vol 20, no 1, (2016) 149-156.

[34] Z. Z. Chowdhury, S. M. Zain, R. A. Khan, and K. Khalid, "Linear Regression Analysis for Kinetics and Isotherm Studies of Sorption of Manganese (II) Ions Onto Activated Palm ash from Waste Water," Oriental Journal of Chemistry, vol. 27, no. 2, (2011) 405-415.

[35] Y. Yu, Y.-Y. Zhuang, and Z.-H. Wang, "Adsorption of Water-Soluble Dye onto Functionalized Resin," Journal of Colloid and Interface Science, vol. 242, no. 2, pp. 288-293, 2001/10/15 2001

[36] M. Dakiky, M. Khamis, A. Manassra, and M. Mer'eb, "Selective adsorption of chromium(VI) in industrial wastewater using low-cost abundantly available adsorbents," Advances in Environmental Research, vol. 6, no. 4, (2002) 533-540

[37] P. R. Rout, P. Bhunia, R. R. Dash, "Evaluation of kinetic and statistical modelsfor predicting breakthrough curves of phosphate removal using dolochar-packed columns", Journal of Water Process Engineering, vol. 17, (2017) 168–180

[38] O. Hamdaoui, "Dynamic sorption of methylene blue by cedar sawdust and crushed brick in fixed bed columns", Journal of Hazardous Materials, vol. 138, no. 2, (2006) 293–303

[39] A. A. Ahmad, B. H. Hameed, " Fixed-bed adsorption of reactive azo dye onto granular activated carbon prepared from waste", Journal of Hazardous Materials, vol. 175, no. 1 - 3, (2010) 298 - 303

Table 1: Adsorption parameters of three different isotherm models for emulsified oil removal from synthetic produced water using G and GM

Adsorption Isotherm Model	**Parameters**		
		G	**GM**
Langmuir Isotherm	b (L/mg)	0.0190 (±0.001)	0.0256 (±0.0013)
	q_m (mg/g)	130 (±3.9)	62.5 (±2.1)
	R^2	0.988	0.981
Freundlich Isotherm	k_f ($mg^{(1-1/n)}L^{1/n}/g$),	5.290 (±0.158)	2.849 (±0.086)
	N	0.60 (±0.017)	0.64 (±0.018)
	R^2	0.993	0.997
Temkin Isotherm	B (J/mole)	23.00 (±0.68)	12.14 (±0.34)
	K_T (L/mg)	0.28 (±0.084)	0.066 (±0.019)
	R^2	0.962	0.97

Table 2: Oil adsorption capacities of different adsorbents [18]

Adsorbent Used	Type of Oil Adsorbed	Adsorption Capacity mg/g
Carbon nanotubes sponges	Oil spills	92.300
Magnetic expanded graphite	Crude oil	35.720
Acetylated rice straw	Machine oil	24.000
Hydrophobic silica aerogels	Liquid oil	15.100
Modified oil palm leaves	Crude oil	1.200
Barley straw	Canola oil	0.613
	Standard mineral oil	0.583
Egg shells	Crude oil	0.109
Organo-clay	Emulsified oil	0.067
Modified bentonite	Emulsified oil	0.049
Graphene	Emulsified oil	0.100
Graphene magnetite	Emulsified oil	0.085

Table 3: Adsorption parameters of pesudo-first order and pesudo-second order kinetic models for removal of emulsified oil from synthetic produced water using G and GM

Sr. No.	**Experimental**	**Pseudo-first-order kinetic model**			**Pseudo-second-order kinetic model**		
	q_{exp} (mg/g)	K_I (1/min)	q_{calc} (mg/g)	R^2	K_{II} (g/mg.min)	q_{calc} (mg/g)	R^2
G	45.4 (±1.4)	0.106 (±0.032)	13.8 (±0.42)	0.89	0.020 (±0.001)	45.9 (±1.38)	0.999
GM	29.1 (±0.87)	0.037 (±0.001)	296 (±7.98)	0.73	0.009 (±0.001)	30.3 (±0.91)	0.999

Table 4: Values of n, K_{ad}, Q^T and ΔG' estimated for the adsorption of oil on graphene magnetite at different temperatures.

Temperature (K)	**Sips**				**Freundlich**		**ΔG' (kJ/mol)**
	K_{ad}	**Q^T(mg/g)**	**N**	**$K_f = Q_T/K_{ad}$**	**n**	**K_f***	
298 ± 0.5	0.0246 (±0.0007)	83.6 (±2.5)	0.62 (±0.020)	3401 (±20.49)	0.64 (±0.018)	3917 (±117.5)	-9.2 (±0.2)
303 ± 0.5	0.0240 (±0.0007)	57.9 (±1.7)	0.59 (±0.019)	2415 (±17.78)	0.59 (±0.017)	2376 (±71.31)	-9.4 (±0.3)
313 ± 0.5	0.0160 (±0.0005)	65.4 (±2.0)	0.66 (±0.020)	4082 (±101.9)	0.65 (±0.019)	3820 (±115.9)	-10.8 (±0.3)
323 ± 0.5	0.0108 (±0.0003)	85.5 (±2.6)	0.74 (±0.020)	7913 (±135.5)	0.74 (±0.024)	7639 (±152.8)	-12.2 (±0.4)

*Values of K_f are calculted based on the concentration of adsorbate in mol/L .

Table 5: Themodynamic parameters (adsorption of emulsied oil on graphene magnetite)

ΔG′				ΔH′	ΔS′
298.1 K	303.1 K	313.1 K	323.1 K		
kJ/mol				kJ/mol	kJ/mol.K
-9.2 (±0.2)	-9.4 (±0.3)	-10.8 (±0.3)	-12.2 (±0.4)	27.6 (±0.8)	0.123 (±0.004)

Table 6: Adsorption parameters of five different column models for emulsified oil removal from synthetic produced water using GM (column studies)

Adsorption Isotherm Model	**Parameters**			**R^2**
Thomas	K_{TH}	ml/mg.min	$1.5*10^{-2}$ ($\pm 4.0*10^{-4}$)	0.995
	q_o	mg/g	183.4 ($\pm$5.5)	
Yan et al.	K_y	ml/mg.min	3.08 ($\pm$0.092)	0.591
	q_o	mg/g	134.9 ($\pm$4.0)	
Clark	A	-	17.4 ($\pm$0.52)	0.975
	R	1/min	$2.0*10^{-3}$ ($\pm 6.0*10^{-5}$)	
Bohart & Adams	K_{ab}	L/mg.min	$5.0*10^{-6}$ ($\pm 1.5*10^{-7}$	0.949
	N_o	mg/L	$1.7*10^{5}$ ($\pm 5.1*10^{3}$)	
Yoon & Nelson	T	min	$1.6*10^{3}$ ($\pm 4.1*10^{1}$)	0.995
	K_{yn}	1/min	$3.0*10^{-3}$ ($\pm 9.0*10^{-5}$)	

Table 7: The variation in Thomas isotherm model parameters at different flowrates and bed height.

Flowrate	Bed Height	K_{TH}	q_o	R^2
ml/min	cm	ml/mg.min	mg/g	
0.4	2	$1.5*10^{-2}$ ($\pm 4.0*10^{-4}$)	183.4 ($\pm$5.5)	0.995
0.4	1.5	$2.0*10^{-2}$ ($\pm 3.7*10^{-4}$)	173.6 ($\pm$4.6)	0.983
0.8	1.5	$3.0*10^{-2}$ ($\pm 4.1*10^{-4}$)	139.8 ($\pm$3.8)	0.983